KSCE Journal of Civil Engineering (2020) 24(2):657-669
DOI 10.1007/s12205-020-2054-2

pISSN 1226-7988, eISSN 1976-3808
www.springer.com/12205

Tunnel Engineering

3D Discrete Element Method Modelling of Tunnel Construction Impact on an Adjacent Tunnel

Lin Wu[a], **Xiedong Zhang**[a], **Zhihua Zhang**[b], **and Weichen Sun**[c]

[a]*School of Transportation, Wuhan University of Technology, Wuhan 430063, China*
[b]*Changjiang River Scientific Research Institute of Changjiang Water Resources Commission, Wuhan 430010, China*
[c]*Hebei Chenya Technology Co. Ltd., Shijiazhuang 050056, China*

ARTICLE HISTORY

Received 17 October 2018
Revised 18 April 2019
Accepted 22 November 2019
Published Online 3 January 2020

KEYWORDS

Twin tunnels
Construction influence
Discrete element method
Displacement
Porosity variation
Influenced area
Reinforcement measure

ABSTRACT

Closely-spaced side-by-side mechanized twin tunnels are commonly used in urban metro transit systems. The aim of this paper was to investigate the influence of tunnel construction on an adjacent existing tunnel using the 3D discrete element method (DEM) and propose a new method to protect the existing tunnel. The first tunnel at the left side was initially included in the DEM model. The construction of the second adjacent tunnel at the right side was then modelled in phases. Displacement, stress variation, porosity variation, and coordination of surroundings of the first tunnel were investigated. The results showed that the excavation of the second tunnel had a great negative impact on the existing tunnel surroundings when the distance of twin tunnels was less than the diameter of the tunnel. The maximum horizontal displacement occurred at the angle of 45° and was equal to 103 mm. The influenced area of the existing tunnel is the surroundings between the tunnel crown and the spring line on the second tunnel side near the tunnel lining. The composite reinforcement method consists of pasted fiber reinforced plastic (FRP) sheet method and grouting in a specific area; thus, the structure safety and the normal operation of the existing tunnel nearby can be guaranteed. The protective method can give reference for similar project.

1. Introduction

Mechanized twin tunnels are indispensable parts of the urban metro transit system and widely constructed to satisfy the increasing transportation demands. The design of twin tunnels is often challenging due to the complex behavior of surrounding soils and the interaction between closely spaced twin tunnels (Abd-el.rahim et al., 2015; Fang et al., 2016). In engineering projects, the side-by-side twin tunnel is widely used, and its layout leads to the smallest ground movement compared to other layouts, such as vertical aligned and diagonal vertical aligned twin tunnels. Typically, laboratory model test and numerical simulation are used in the design.

Laboratory model tests have been widely used and often provide reliable data to assess the behavior of twin tunnels during the construction process, replacing field prototype monitoring in most cases. Chapman et al. (2007) conducted a small-scale laboratory test at 1 g. The tested tunnel diameter was 50 times smaller than that of the real tunnel. An auger type cutter was used in Champman's test to excavate the tunnel and a shield to support the surroundings during the tunnel construction. The observed ground movements are similar to the results of the full-scale case studies. Choi and Lee (2010) simulated twin tunnel excavation model tests by a sharp drill to quantify the displacement and crack propagation of surrounding soils. To model the Chengdu Metro Line 1 tunnel construction, a small-scale (1/12) model was constructed by He et al. (2012) using a small-scale (1/12) earth pressure balance (EPB) model shield machine. The test results showed that settlements across the tunnels in the physical model and field test were similar. Li et al. (2014) carried out a centrifuge model test of vertically aligned twin tunnels by simulating the tunneling process in three excavation steps. The results showed that the surroundings between the axis of the new shield tunnel and the existing tunnel heave when the distance between the twin tunnels was smaller than 39 m. They noted that it was difficult to accurately simulate the excavation process of

CORRESPONDENCE Lin Wu wl256724@whut.edu.cn School of Transportation, Wuhan University of Technology, Wuhan 430063, China

the real tunnels in the centrifuge model test. Shahin et al. (2016) used the model test to investigate the realistic ground behavior of existing building and tunnel during tunnel excavation. Qiu et al. (2017) investigated that the stratum deformation distribution near the vault changes from a single-peak V shape to a double-peak W shape during the increase of tunnel spacing in the comprehensive centrifuge tests. Inadequate representation of the real tunnel excavation in the test model could result in large disturbances to the surrounding soils and, in turn, unrealistic test results.

Numerical simulation has a variety of important branches including finite element method (FEM), Finite difference method (FDM), Mesh-free method (Rabczuk and Belytschko, 2004; Arun et al., 2010; Ostermann et al., 2013; Michel et al., 2017), and discrete element method (DEM). Soils movements (Addenbrooke and Potts, 2001; Chen et al., 2012; Abd-el.rahim et al., 2015) and mechanical behaviors of tunnel lining (Kim, 2004; Chehade and Shahrour, 2008) are two main research aspects of FEM method. FLAC^{3D} finite difference element programme is also widely used as an FDM method. Do et al. (2014; 2015; 2016) have simulated mechanized twin tunnels in the soft ground using FLAC^{3D}. The influence of different distance of twin tunnels in cross-section and longitudinal directions during tunnel excavation are discussed. Chakeri et al. (2015) have focused on the influence of different soils conditions in the longitudinal direction of tunnel excavation and mixed ground in tunnel face by FLAC^{3D}. While the simulation of dynamic process using FEM and FDM during tunnel excavation has not been conducted, causing the inaccuracy of simulating the discrete features around the twin tunnels.

DEM has been increasingly used to model the soil mass more realistically as individual particles (Cundall, 1971; Cundall and Strack, 1979). Particle flow code (PFC) is one of the most commonly used software packages that is based on DEM (Itasca, 2008). The PFC overcomes the macro-continuity assumption and has great advantages for modeling complicated problems in solid mechanics and granular flow. Funatsu et al. (2008) conducted numerical simulations using PFC2D to assess the effects of ground supports and reinforcements on tunnel stability. He and Manafi (2012) studied the behavior of ground arches at the microscopic level for the mechanized twin tunnels of the Chengdu Metro Line 1 project using PFC2D. Oliaei and Manafi (2015) studied the impact of the relative position and construction procedure of twin tunnels using PFC2D. To date, previous DEM research on twin tunnels has been limited to two-dimensional analysis using PFC2D and fails to capture the out-of-plane effects and realistically simulate the dynamic construction process of twin tunnels. As such, three-dimensional DEM modelling is needed to assess the impact of tunnel constructional on an existing adjacent tunnel.

With this background, this paper presents the development of a PFC3D model of twin tunnels consisting of seven segments to investigate the impact of the construction of a second tunnel on an existing adjacent tunnel and proposes a new method to protect the existing tunnel. Construction of the second tunnel was simulated after the first tunnel achieved a numerically stable state to reduce the disturbance due to the construction of the first tunnel. An accelerate excavation speed in the numerical simulation process is considered to reduce the computational time. The impacts of the construction of the second tunnel on the first tunnel surroundings, including displacement, stress variation, porosity variation, and coordination number, are assessed. Coordination number is the average number of contact points per particle within a specified volume (i.e., within the measurement sphere). Based on the analysis results, protective measures for the affected zone, referred to here as the influence area, of the first tunnel liner are proposed. The comprehensive investigation of the first tunnel's behavior and the proposed protective measures could guarantee normal operations of the existing tunnel during the excavation of the second tunnel, which can give reference for similar project.

2. Numerical Model

2.1 Relevant Macro-Parameters

Wuhan Metro Line 7 was chosen for the reference project, which

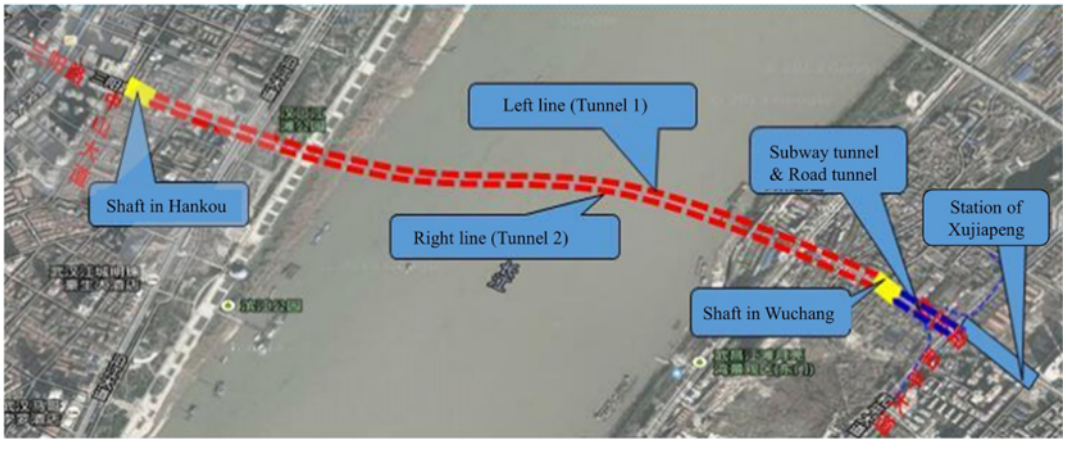

Fig. 1. The Aerial View of Twin Tunnels in the First Stage of Wuhan Metro Line No. 7 Project (Tunnel 1 denotes the first (left) tunnel and Tunnel 2 denotes the second (right) tunnel.)

began in December 2013 and is still ongoing. An aerial view of twin tunnels in the first stage of the Wuhan Metro Line No. 7 project is shown in Fig. 1. Tunnel 1 denotes the first tunnel and Tunnel 2 denotes the second tunnel. The project consists of the construction of twin tunnels under the Yangtze River. The tunnels are the first shield twin tunnels where the city road and the rail transportation are constructed in the same tunnel section, which has a 15.2 m outer diameter of lining in this part and a 6.2 m outer diameter of lining in other part. The distance between the two tunnels is small and less than one diameter in some places. For this reason, the construction of the second tunnel would influence the existing tunnel, causing noticeable deformations and cracks in the lining and surroundings of the existing tunnel.

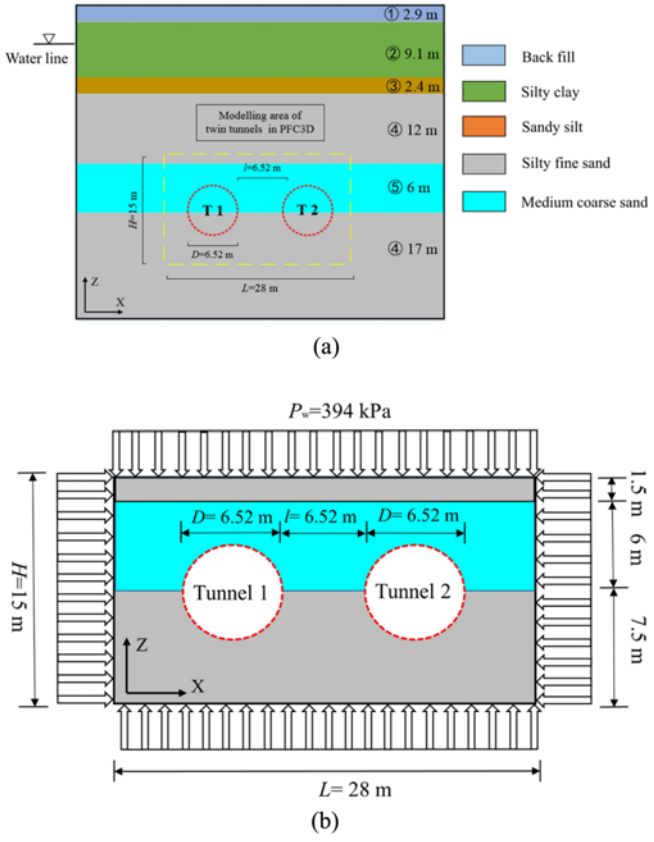

Fig. 2. Diagram of Specified Cross Section of Twin Tunnels in the First Stage of the Wuhan Metro Line No. 7 Project: (a) Specified Cross Section of Twin Tunnels in the Engineering Project, (b) Simplified Cross Section of Twin Tunnels in PFC3D Model (T 1 and Tunnel 1 are short for the first tunnel, T 2 and Tunnel 2 are represent for the second tunnel; D is the diameter of tunnel, l is the clear distance of twin tunnels, L and H are the length and height of model, respectively; P_w is the simplified hydrostatic pressure applied on the boundary of numerical model)

An outer diameter for the tunnel liner of 6.2 m is considered for the analysis in this paper as tunnels with diameters of 6.0 m to 6.5 m are common in engineering projects. By considering the construction gap, the excavation diameter for the real twin tunnels is 6.52 m as shown in Fig. 2(a), which is slightly larger than the outer diameter of the modelled twin tunnels of 6.2 m. In this paper, the outer diameter of the lining of Tunnel 1 and the excavation diameter of Tunnel 2 are both 6.52 m, and the spacing between the sides of the tunnels is 6.52 m. The minor difference between the real diameter of 6.2 m (the lining of Tunnel 1) and the supposed diameter of 6.52 m is small; thus the effect can be ignored. For simplicity, the soils far away from the twin tunnels were not included in the numerical model, and a confining pressure was applied to the model boundaries to simulate the lateral pressure from the surroundings. A simplified cross-section of the PFC3D model is shown in Fig. 2(b). The size of the model was determined in consideration of the computational time and to minimize boundary effects (Maynar and Rodrigues, 2005). The confining pressure for the model was taken as an equivalent hydrostatic pressure, which was taken as the average of water and soil pressures acting on the six model boundaries. The simplified equivalent hydrostatic pressure $P_w = 394$ kPa and was applied to six boundary walls of the model.

Physical and mechanical properties of the soil strata in the DEM model are shown in Table 1 (China Fourth Railway Survey and Design Group Co., Ltd, 2013). The elasticity modulus (E) of the soils are three times the compressive elastic modulus (E_s) (Yu, 2014).

2.2 Determination of Micro-Parameters

Material parameters, element size and distribution have influence on the parameter behaviors. Uncertainty analysis (Vu-Bac et al., 2016; Hamdia et al., 2017) could show the influence of all uncertain input parameters including such as element size and distribution. As material parameters have the most important influence on the behaviors of material, the element size and distribution keep the same value and their influence have been ignored.

To date, there is no complete theory that can predict macroscopic behaviors from microscopic properties and geometry. As a result, the determination of particle and contact parameters is critical. There are two methods for calibration of the micro-mechanical parameters of soils: one is based on comparison of laboratory experiments and DEM tests, and when the stress-

Table 1. Physical and Mechanical Properties of the Soil Strata

ID	Name	E (MPa)	γ (kg/m^3)	W (%)	c (kPa)	φ (°)	v
④	Silty fine sand	65.7	2,039	20.4	7.0	31.9	0.3
⑤	Medium coarse sand	39.9	2,161	22.2	2.0	40.0	0.3

Note: E = elasticity modulus; γ = unit weight; w = moisture content; c = cohesion; φ = friction angle; v = Poisson's ratio

strain curves obtained from laboratory experiments and DEM simulations are in agreement under different confining pressures, (Maynar and Rodrigues, 2005; Zhang et al., 2011; Zhang et al., 2018) the calibration process to obtain the micro-mechanical parameters is completed; the other is to determine the micro-mechanical properties based on matching the macro-behaviour (such as, elastic modulus, cohesion, friction angle, Poisson's ratio and so on) to established correlations (Wang et al., 2011; Wang et al., 2018), and the advantages of this method are that the goal of the calibration process is more explicit, and it does not require undertaking time-consuming laboratory experiments. In this paper, the second method was used to determine the micro-parameters of the surrounding soils.

A series of numerical triaxial tests were conducted to obtain the target micro-parameters for the silty fine sand and the medium coarse sand (see Table 1). Fig. 3 shows the triaxial numerical model used for the calibration and the compressing process for the numerical triaxial test. The compressing process was conducted by moving the upper and lower "walls", which are rigid loading plates with much larger stiffness of particles inside. The stiffness of the side wall is approximately equal to the stiffness of the particles in order to simulate the rubber membrane in the physical triaxial test. Three different confining pressures of 100 kPa, 300 kPa and 500 kPa, were used.

The linear contact model (Itasca, 2008) is used for the silty fine sand and the medium coarse sand. The calibration process is illustrated in Fig. 4. The micro-parameters are contact Young's modulus (E_c) or contact normal stiffness (k_n), the ratio of contact normal to shear stiffness (k^*) and contact friction coefficient (μ). The macro-parameters are elastic modulus (E, E'), cohesion (c, c'), friction angle (φ, φ'), and Poisson's ratio (v, v'). In particular, c' and c represent total stress in this paper. c' is the equivalent value obtained from PFC3D as shown in Fig. 4.

The micro-parameters were determined by first assuming initial values for each micro-parameter. The initial value of E_c is set as the value of the elasticity modulus (E) (Table 1). The initial value of k^* is set as 1.0. The initial value of the friction coefficient is calculated by using Eq. (1). An initial model was undertaken. The stress-strain curve and Mohr's stress circle for the modelled soil were computed and used to analyze the corresponding macro-parameters. The process was then repeated by using different sets of micro-parameters until the target macro-properties were achieved.

$$\mu = \tan\varphi \tag{1}$$

Taking the medium coarse sand as an example, the deviatoric stress versus axial strain curve and Mohr's stress circles for the three different confining pressures are shown in Fig. 5. The elasticity modulus (E') was determined from the deviatoric stress versus axial strain curve corresponding to the point of 50% of the maximum deviatoric stress as shown in Eq. (2) (Ming et al., 2017):

$$E' = E'_{50} = \frac{\sigma_{max}/2}{\varepsilon} \tag{2}$$

where E'_{50} is the elastic modulus at 50% of the maximum deviatoric stress, taken for the case of confining pressure of 300 kPa, which is approximately equal to the in-situ hydrostatic pressure; σ_{max} is the maximum value of stress.

The Passion's ratio (v'), obtained for the case of confining pressure, was 300 kPa. Cohesion (c') and friction angle (φ') were obtained by using Mohr's circle of stress. In this case, the macro-parameters, which are calculated from the micro-parameters in DEM calibration model, is close to the macro-parameters

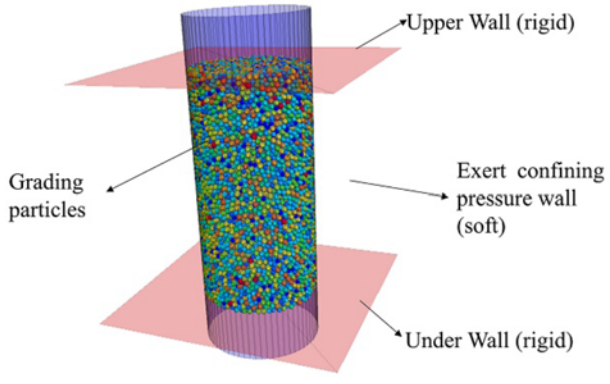

Fig. 3. Calibration Model in Numerical Triaxial Test

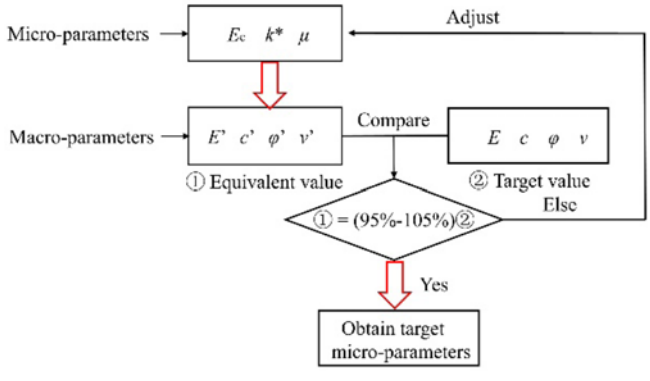

Fig. 4. Calibration Process for Sandy Soils in Numerical Triaxial Test

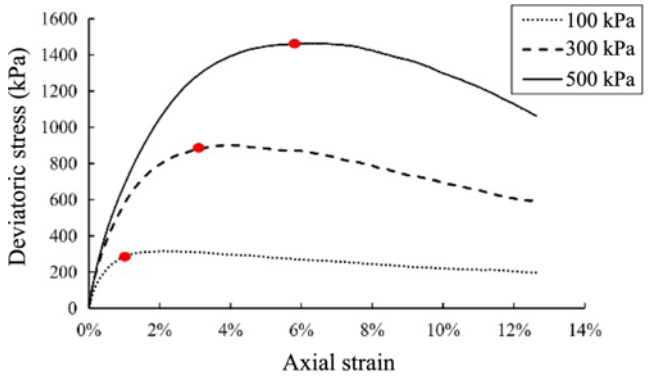

Fig. 5. The Deviatoric Stress versus Axial Strain Curve of Medium Coarse Sand under Different Confine Pressures of 100, 300, 500 kPa

Table 2. Micro-Parameters of Each Soils Stratum

No.	Test A	Test B	Test C	Test D
Soil type	Silty fine	Silty fine	Medium coarse	Medium coarse
Size of model (m) (Diameter × Height)	5 × 10	9 × 18	5 × 10	9 × 18
r (m)	0.1 – 0.12	0.15 – 0.24	0.1 – 0.12	0.15 – 0.24
Number of particles	22,156	22,111	22,156	22,111
E_c (Pa)	2.146×10^8	2.212×10^8	5.985×10^7	5.852×10^7
k^*	1.0	1.0	1.0	1.0
γ(kg/m^3)	1043	1043	1161	1161
μ	0.51	0.51	0.7	0.726

Note: r = radius of particles; E_c = contact Young's modulus; k^* = the ratio of contact normal to shear stiffness; γ = unit weight; μ = contact friction coefficient

obtained from engineering document of Wuhan Metro Line No. 7 project. For this reason, the corresponding micro-parameters of medium coarse sand (radius from 0.15 – 0.24 m) can be used in twin tunnels model. After calibration, the micro-parameters of each soil strata in different sizes are shown in Table 2.

The choice of particle size is based on the existing research (Maynar and Rodrigues, 2005; Chen et al., 2011), which recommended the ratio of the tunnel diameter to the particle mean diameter no less than 10. The sizes of the triaxial model should be greater than 10 times the largest grain diameter (Maynar and Rodrigues, 2005). Four groups of tests from Test A to D were conducted as shown in Table 2.

Taking the medium coarse sand of radius from 0.15 – 0.24 m (Test D in Table 2) as an example, the deviatoric stress versus axial strain curve under the three different confining pressures are shown in Fig. 5. In this case, the macro-parameters which is calculated from the micro-parameters in DEM calibration model is close to the macro-parameters obtained from engineering document of Wuhan Metro Line No. 7 project. For this reason, the corresponding micro-parameters of medium coarse sand (radius from 0.15 – 0.24 m) can be used in twin tunnels model. After calibration, the micro-parameters of each soil strata in different sizes are shown in Table 2.

2.3 Twin Tunnels Model

2.3.1 Initial Model

The size of the twin tunnels model is 28 × 15 × 10.5 m^3 ($L \times H \times W$) and the perspective view of the initial model is shown in Fig. 6. The first tunnel at the left side was initially included in the DEM model. The construction of the second adjacent tunnel at the right side was then modelled in phases. Smaller diameter particles were used in the extra excavation region of Tunnel 2, which has a radius of R + 0.2 (m). The smaller particles were used to reduce the gap between the shield machine and soil particles, providing more accurate results. The "wall" command is used to generate the Tunnel 2 shield machine and Tunnel 1 lining. A very large stiffness was used for the "walls" to provide rigid supports. The length and diameter of the shield machine of

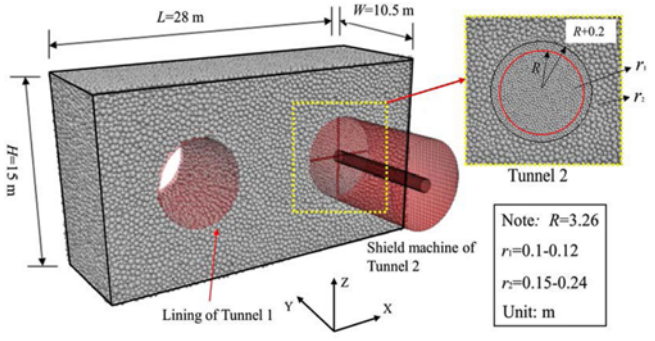

Fig. 6. Perspective View of the Twin Tunnels Model in PFC3D (R is the radius of Tunnel 2 excavation area; r_1 and r_2 are the radii of particles around Tunnel 2.)

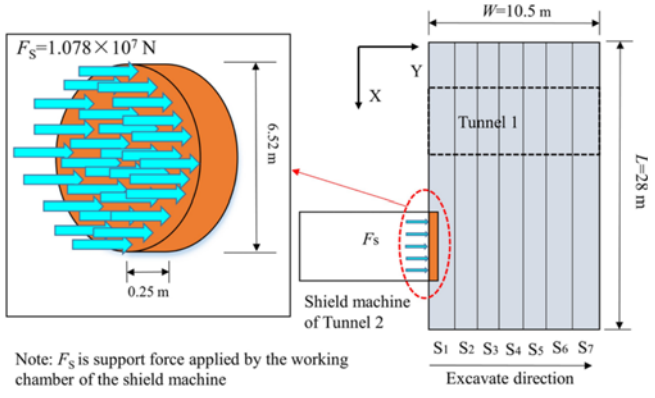

Fig. 7. Support Force Applied by the Working Chamber of Tunnel 2 Shield Machine (F_s is applied to the orange cylindrical region.)

Tunnel 2 are 10.5 m and 6.52 m, respectively.

Support force applied by the working chamber of the Tunnel 2 shield machine is shown in Fig. 7. The total support force applied by the working chamber of the shield machine is F_s = 1.078 × 10^7 N (Jin et al., 2018). In the PFC3D model, this force can be simulated by an equivalent force that was applied to the particles within a specified range which based on the cross-section size of the shield machine. The specified range, which is a cylindrical region, is with a radius of 3.26 m and a width of

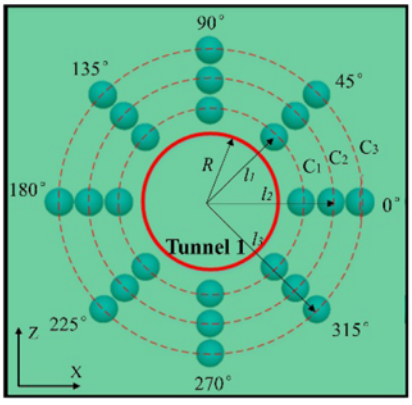

Fig. 8. The Distribution of the Measurement Points and Spheres in the Segment 4 (S_4) Surroundings of Tunnel 1

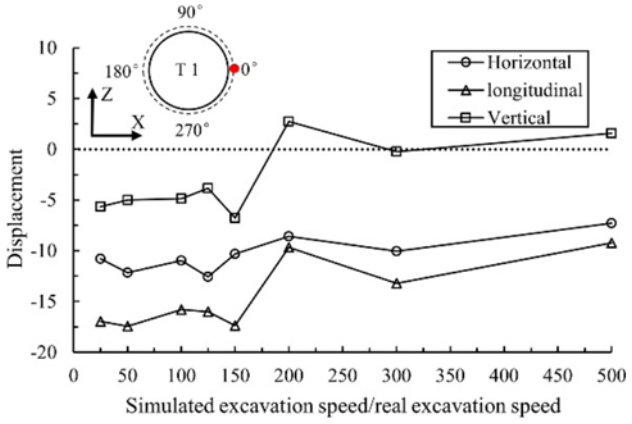

Fig. 9. The Displacement of 0° in Horizontal, Longitudinal and Vertical Directions in Different Ratios of Simulated Excavation Speed/ Real Excavation Speed (unit: mm)

0.25 m. The radius of this cylinder is based on the size of the shield machine and the width of it is based on the width of one layer of particles in front of the shield machine.

During Tunnel 2 excavation, the shield machine then moves forward and rotates simultaneously. The particles near excavation poles were scraped as the machine advances and then were deleted after entering of shield machine. The cylindrical region of applied support force advanced as the excavation went forward. The seven tunnel segments used in the model are referred to as S_1 to S_7.

Before tunnel excavation, measurement points are specified to record the displacements, and measurement spheres are set to calculate the average macro-parameters (stresses, porosity, and coordination number) within the volume of each sphere. The locations of the measurement points and spheres at S_4 near Tunnel 1 are shown in Fig. 8. C_1, C_2, and C_3 represent the inner, middle, and outer measurement circles, respectively.

2.3.2 Excavation Speed in Discrete Element Method

The actual rotary speed and the velocity of the shield machine are 1 rad/min and 50 mm/min, respectively (China Fourth Railway Survey and Design Group Co., Ltd, 2013). If simulate the excavation in this velocity in PFC3D, a single model run would take several months. To overcome this problem, researchers used accelerated excavation speeds in PFC2D and PFC3D models to reduce the computational time in existing studies (Chen et al., 2011; Zhang et al., 2011; Jiang and Yin, 2014).

In this paper, the model optimal excavation speed was determined based on a sensitivity analysis using eight different excavation speeds of 25, 50, 100, 125, 150, 200, 300, and 500 times the real excavation speed. Half of a segment is excavated in each model. The displacements of the particles on the right side (0°) are shown in Fig. 9. As can be seen, the displacements in the horizontal, longitudinal, and vertical directions are almost the same when the excavation speed is 25 – 150 times the real excavation speed. In PFC, the timestep is the real-time simulated per numerical step. The larger the timestep is, the longer the simulated time per step is. As the ratio of simulated excavation speed over real excavation speed increases, the timestep becomes smaller, thus, the total computation time increases. This can be attributed to the larger dynamic effects for the faster excavation speeds in DEM.

Based on the results of this analysis, it was determined that excavation speed equal to 100 times the real speed would results in optimal computation time without compromising the accuracy of the simulations. Using this excavation speed, the average time necessary for one simulation is approximately three weeks, using a 3.4 GHz Core i7 CPU and 8Gb RAM computer.

2.3.3 Simulations Sequence

Step1: Conduct numerical triaxial test for the silty fine sand and the medium coarse sand, and obtain the micro-mechanical parameters.

Step2: Setup the initial model of the twin tunnels and use the micro-parameters from Step 1 in the model. This includes setting up the soils, the boundaries, Tunnel 1 lining, and the shield machine for Tunnel 2.

Step3: Specify measurement points and spheres around Tunnel 1 at segment 4 (S_4) to obtain initial displacements, stresses, porosities, and coordination numbers.

Step4: Zero the initial displacements before Tunnel 2 excavation. The rotational speed of Tunnel 2 machine in the numerical model is then set to 100 rad/min and tunnel advancement speed is set to 0.083 m/s.

Step5: Excavate Tunnel 2 from S_1 to S_7 continuously. The simulation is completed at the end of the tunnel excavation.

3. Results and Discussion

In order to understand the behaviors of the existing tunnel (Tunnel 1) during the construction of the adjacent tunnel (Tunnel 2), it is important to assess the displacement, stress variation, porosity variation, and coordination of Tunnel 1 surroundings. These variations were determined at the middle of S_4 of Tunnel

1. Based on the results, the affected area around Tunnel 1 can be determined. To ensure the safe operation of Tunnel 1 during Tunnel 2 excavation, a method to protect Tunnel 1 liner is recommended for consideration in tunnel design and construction.

3.1 Construction Influence

3.1.1 Displacement

Figures 10(a) – 10(c) illustrates the displacement of Tunnel 1 surroundings in the final excavation stage of Tunnel 2 (S_7). The displacement in horizontal, longitudinal, and vertical directions are larger in the side near the excavation area while smaller in the side far away from the excavation area. The maximum values of horizontal, longitudinal, and vertical displacement are 103, 13, and 81 mm, respectively. The horizontal displacements are the largest while the longitudinal displacements are the smallest. The analysis implies that the longitudinal displacement may be ignored in a design whose value is about 10% of horizontal displacement.

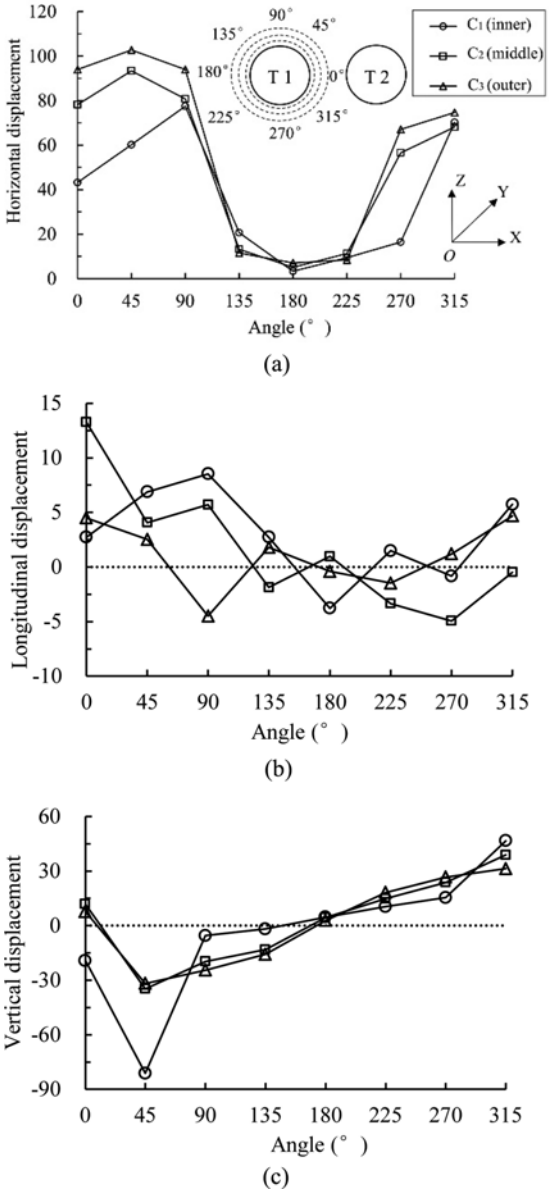

Fig. 10. Displacement of Tunnel 1 Surroundings in the Tunnel 2 Excavation Stage of S_7 in Different Directions: (a) Horizontal, (b) Longitudinal, (c) Vertical (T 1 and T 2 denote the first and second tunnel, respectively) (unit: mm)

Horizontal displacements are always positive, which implies the surroundings of Tunnel 1 have a tendency to move to the right direction during Tunnel 2 excavation. The displacement of particles between the two tunnels in the Tunnel 2 excavation stage of S_7 is shown in Fig. 11. The particles showed in the figure are in segment 4 (S_4) of twin tunnels. The results show that all the particles have the same tendency to move in the horizontal direction. The maximum horizontal displacement occurs at the angle of 45°, and is equal to 103 mm.

Vertical displacements have different directions which the values may be positive or negative (see in Fig. 10(c)). The positive value represents the upward displacement while the negative value means downward displacement. The surroundings upper the horizontal centerline of tunnels move downwards whilst the surroundings below the horizontal centerline of tunnels move upwards due to the unloading effect (Jiang and Yin, 2012) of Tunnel 2 excavation. The vertical displacement of particles between two tunnels in segment 4 (S_4) is shown in Fig. 11. The particles above the horizontal centerlines of tunnels move downwards, while the particles below the horizontal centerlines move upwards.

As expected, the horizontal displacements in the side near the excavation area increase from inner to outer measurement circles (from C_1 to C_3); this can attribute to the distance between the measurement points and excavation area decrease from measurement circles C_1 to C_3. The results show that the horizontal displacement of Tunnel 1 surroundings is directly affected by Tunnel 2 excavation. However, the vertical displacements in the side near the excavation area decrease from measurement circles C_1 to C_3. The larger vertical displacements in the inner measurement

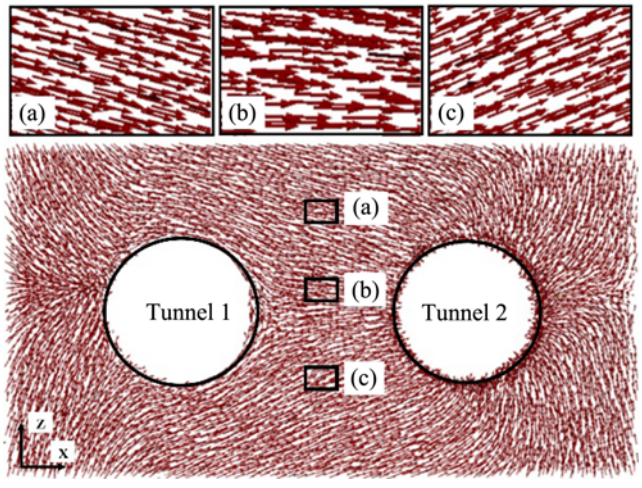

Fig. 11. The Displacement Direction of Particles between Twin Tunnels in Segment 4 (S_4) in the Tunnel 2 Excavation Stage of S_7

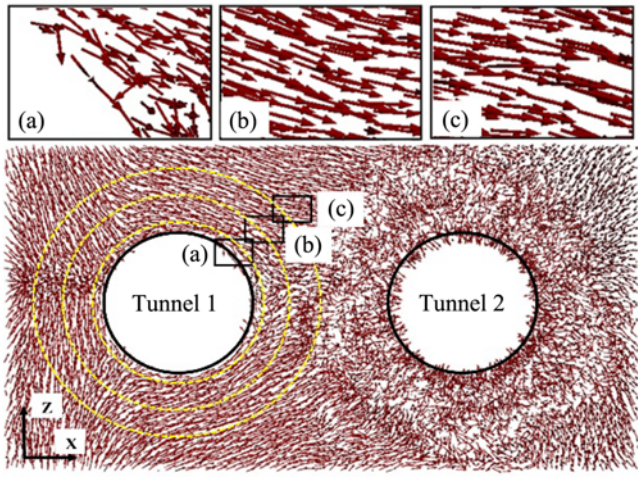

Fig. 12. The Velocity Direction of Particles in Segment 4 (S_4) at Measurement Circles C_1 to C_3 of 45° in the Tunnel 2 Excavation Stage of S_7 (Tunnel 1 and Tunnel 2 denote the first and second tunnel, respectively)

circle of C_1 are due to the confining effect of the Tunnel 1 lining and the disturbance caused by Tunnel 2 excavation. At the inner measurement circle of C_1, the particles near the tunnel lining slide as there are fewer particles at these locations to provide sufficient support. Arrows representing particle velocities at 45° angle for measurement circles C_1 to C_3 are shown in Fig. 12. It can be seen that the arrows for Figs. 12(b) and 12(c) are almost the same, while these in Fig. 12(a) are different because of the proximity to the tunnel lining. The velocity arrows at 45° angle for inner measurement circle C_1 follow the edge of Tunnel 1 lining.

The results show that the largest horizontal displacement occurs at outer measurement circle C_3 and the largest vertical displacement is at inner measurement circle C_1. The horizontal displacement at C_3 and the vertical displacement at C_1 during Tunnel 2 excavation are shown in Figs. 13(a) and 12(b), respectively. During the advancement of Tunnel 2 excavation, the horizontal and vertical displacements of the soils around Tunnel 1 increase gradually. The measurement points in other measurement circles have a similar moving tendency during Tunnel 2 excavation.

As a whole, the results shown in Figs. 11 to 14 indicate that the highest impact of Tunnel 2 construction is within the zone between angles of 0° and 90° (i.e., from the Tunnel 1 crown to the right spring line), with the maximum displacements at angle 45°. The significant sliding and large displacements in this area may cause cracking in Tunnel 1 liner, which can cause leakage and corrosion of the reinforcement. Additional displacement monitoring is recommended at those locations during the construction of the adjacent tunnel.

3.1.2 Stress Variation

In DEM, the average field theory is usually employed to compute stresses in a given volume, such as in a measurement sphere (Itasca, 2008). In order to remove the influence of different depths and orientations, in this paper, changes in horizontal, longitudinal and vertical stresses are normalized by their corresponding initial values (Zhang et al., 2011; Jiang and Yin, 2012). In other words, the variation of horizontal stress ($\Delta\sigma_x$) is divided by initial horizontal stress (σ_{x0}), the variation of longitudinal stress ($\Delta\sigma_y$) is divided by initial longitudinal stress (σ_{y0}), and the variation of vertical stress ($\Delta\sigma_z$) is divided by initial vertical stress (σ_{z0}).

Figures 15(a) to 12(c) show stress ratios in the horizontal, longitudinal and vertical directions around Tunnel 1. Stresses in the three directions on the left side of Tunnel 1 are generally higher than in-situ stresses, which is due to load transfer from the new tunnel to the existing tunnel (Do et al., 2014). During Tunnel 2 excavation, soils in the left side of Tunnel 1 becomes denser. This is associated with the increase in stresses.

However, stresses on the right side of Tunnel 1 generally decrease compared with in-situ condition, expect for σ_z at the angle of 0° of measurement circles C_2 and C_3. The stress decrease on the right side of Tunnel 1 is because of stress relaxation caused by Tunnel 2 excavation. The values of σ_z at angle 0° of measurement circles C_2 and C_3 both increase during Tunnel 2 excavation (see Fig. 14(c)), which is different from the decrease

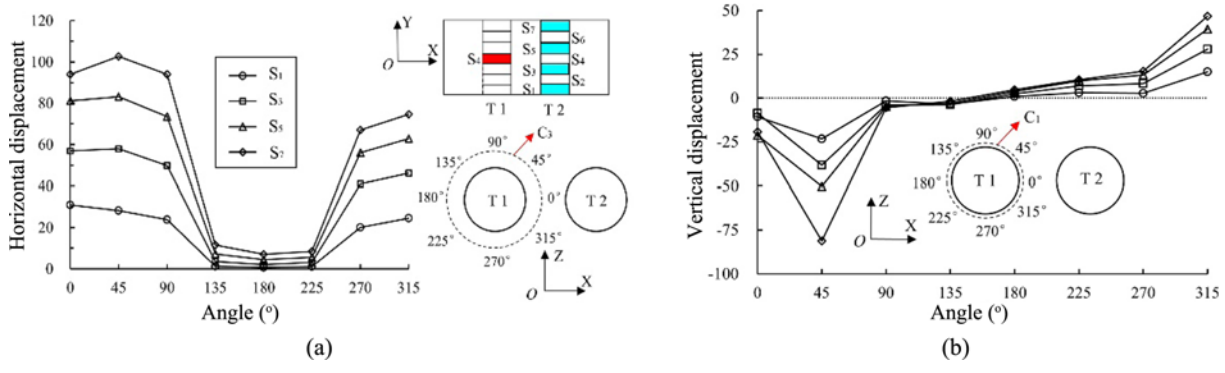

Fig. 13. Displacements of Measurement Circles during Different Excavation Stages of Tunnel 2: (a) Horizontal Displacement at Outer Measurement Circle of C3 , (b) Vertical Displacement at Inner Measurement Circle of C1 (Red rectangle represents the measurement segment of Tunnel 1, blue rectangles represent the different excavation stages of Tunnel 2)

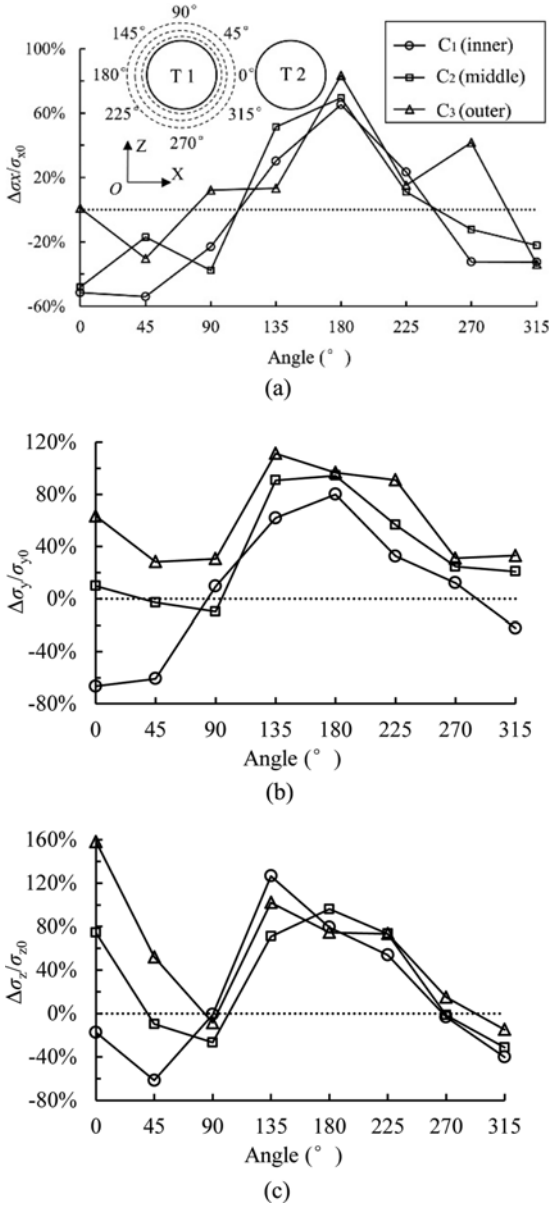

Fig. 14. Stress Variation of Tunnel 1 Surroundings in Different Directions: (a) $\Delta\sigma_x/\sigma_{x0}$, (b) $\Delta\sigma_y/\sigma_{y0}$, (c) $\Delta\sigma_z/\sigma_{z0}$ in the Tunnel 2 Excavation Stage of S_7

trend of stress observed at the other points. This can be attributed to soils above the horizontal centerline of tunnels moving downwards while the soils below the horizontal centerline of tunnels moving upwards (see Figs. 10(c) and 12). This movement towards the middle of the model causes squeezing of the particles and an increase of stress in z-direction. From the middle (C_2) to outer (C_3) measurement circles of Tunnel 1, the squeezing effect becomes more apparent when the measurement spheres closer to the adjacent tunnel.

Stress in the longitudinal direction ($\Delta\sigma_y/\sigma_{y0}$) increase from in-situ conditions at almost all the measurement spheres, except for two measurement spheres at inner measurement circle C_1, between angles 0°and 45° (see Fig. 15(b)). The decrease of $\Delta\sigma_y/\sigma_{y0}$ at C_1 may be the result of particle sliding, which is because there are fewer particles at the locations of C_1 to provide sufficient confinement in the longitudinal direction.

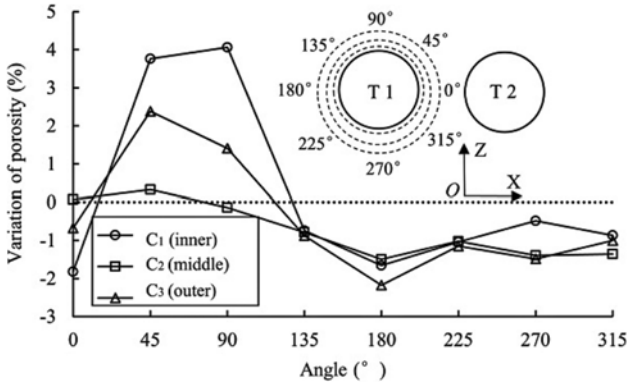

Fig. 15. Porosity Variation of Tunnel 1 Surroundings in the Tunnel 2 Excavation Stage of S_7

3.1.3 Porosity Variation

Variations of porosity near Tunnel 1 were also investigated at Tunnel 2 excavation stage S_7 (see Fig. 15). Soil porosity increases at locations between angles of 45° and 90°. The porosity at the other locations around Tunnel 1 decreases.

As shown in Fig. 15, the change of porosity relative to initial conditions (i.e., before Tunnel 2 excavation) are largest at C_1, followed by C_3 and C_2. Measurement spheres in the outer measurement circle C_3 which near the excavation area and in the inner measurement circle C_1 which near the Tunnel 1 lining also have larger porosity variation. The large changes in porosity at C_1 can be attributed to the collision between the particles and the liner, while the large porosity changes in measurement circle C_3 can be attributed to the proximity to Tunnel 2 excavation, where large excavation disturbances are anticipated. Because the porosity changes in measurement circle C_1 are larger than these at C_3, the collision of the surroundings and the liner is considered the main factor for the observed changes in porosity.

As discussed above, the collision of the soil with the liner causes the soil to become looser, weakening the lining support and decreases its stability. The collision of soil combined with the large displacements between angles of 0° and 90° near Tunnel 1 liner, can cause cracks in the liner, which results in underground water flow and reduced tunnel durability.

3.1.4 Coordination Number

Figure 16 shows the coordination of the soils around Tunnel 1 during Tunnel 2 excavation. The coordination is shown at four angles around Tunnel 1. The variation of the coordination reflects the amount of displacement around Tunnel 1 during Tunnel 2 excavation. Large changes in coordination indicate relatively large displacements.

The largest coordination occurs at inner measurement circles C_1. It is noted that the coordination changes dramatically at

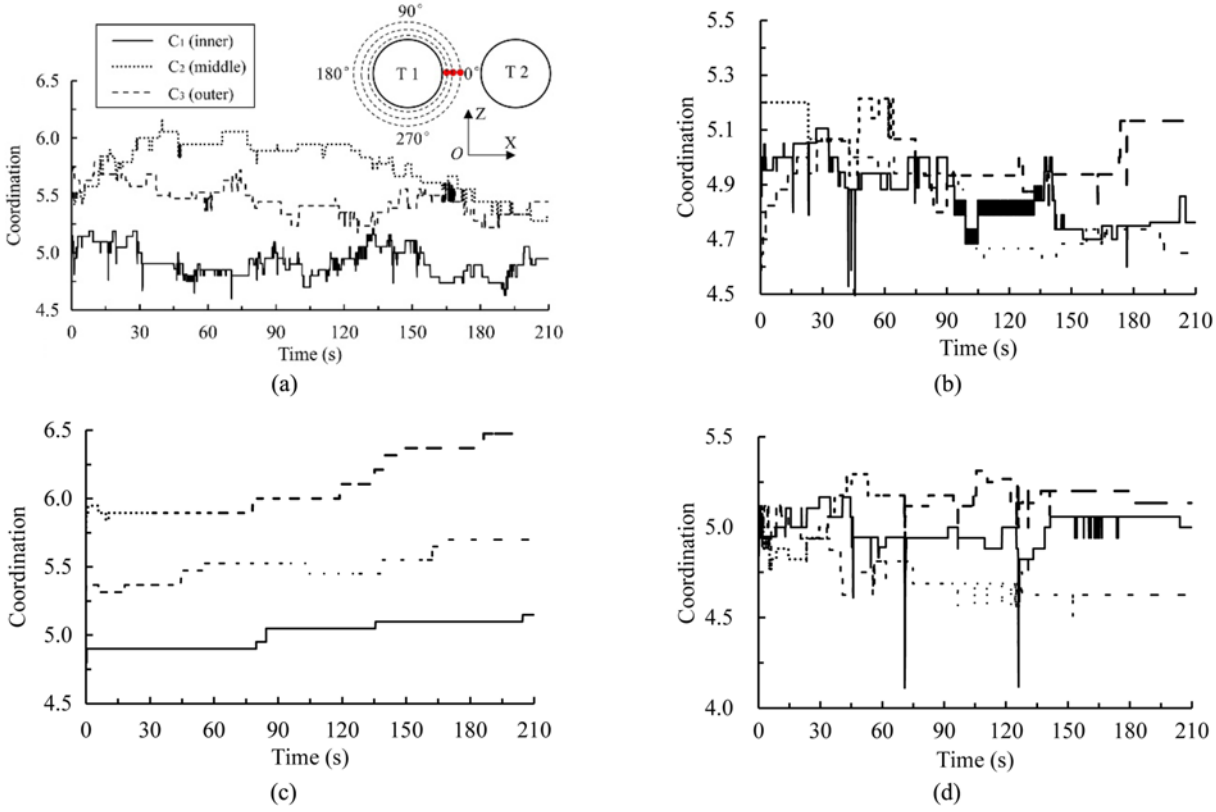

Fig. 16. Coordination of Tunnel 1 Surroundings in Different Angles of: (a) 0°, (b) 90°, (c) 180°, (d) 270° during Tunnel 2 Excavation Process

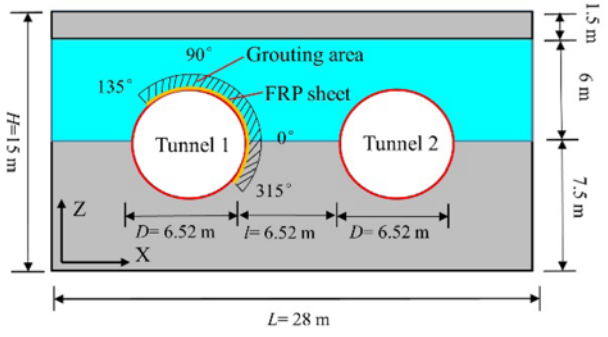

Fig. 17. Diagrammatic Drawing of Composite Reinforcement Method for Tunnel 1 Surroundings

different excavation stages as shown in Figs. 17(b) and 7(d). This can be attributed to the effect of the lining on the surrounding soils. The particles near the tunnel lining become looser during Tunnel 2 excavation (see Fig. 15), which implies a decrease in the coordination for these particles.

Comparing the coordination at 0° (see Fig. 16(a)) and 180° (see Fig. 16(c)), the variation of coordination at 0° are larger than at 180°. This suggests that the closer the distance between measurement spheres and excavation area, the larger the changes in coordination. At 180°, the excavation effect is very small. The small increase in coordination at 180° can be attributed to the compression effect by the boundary confining pressure.

3.2 Influenced Area

Based on the analysis of displacements and changes in stress, porosity, and coordination within the soils around Tunnel 1, it was shown that the impact of Tunnel 2 excavation on Tunnel 1 is highest between the tunnel crown and the spring line on the Tunnel 2 side (from the angle of 0° to 90°). In this region, the largest displacements in the horizontal and vertical directions occur, along with a significant decrease in stress in the three directions. The noted increase of porosity in this region indicates that the soil becomes looser and is less able to provide support. This in line with the significant decrease in coordination in this region. In this section, this region is called the influenced area.

Within the influenced area, cracks in the liner can develop causing leakage of underground water, which can cause tunnel rebar corrosion. The adverse effects of Tunnel 2 excavation can have huge impacts on the durability of Tunnel 1. As such, proper measures should be taken to avoid this damage.

In order to minimize the interaction of the tunnels during the construction process, Li et al. (2014) studied the effect of soil grouting between the two tunnels. They found that the vertical displacement and pore water pressure decrease with the increase of grouting ratio. As a result, they concluded that grouting is an effective measure to mitigate the displacements of the existing tunnel. Chen et al. (2017) studied several tunnel reinforcement methods using pasted fiber reinforced plastic (FRP) sheets, steel plate lining reinforcement and textile-reinforced concrete (TRC). Jin et al. (2018) investigated an in-tunnel grouting method for an

existing upper tunnel during the excavation of the lower twin tunnel. It was found that the grouting protection method can increase the rigidity and control the deformation of tunnel lining, effectively.

The proposed protective method to reduce the negative effect on the influenced area is illustrated in Fig. 17. The composite reinforcement method consists of a Pasted FRP sheet and grouting within the influenced area around the tunnel liner. FRP sheets can be placed at the outer edge of Tunnel 1 liner between angles of 135° to 315°, which extends slightly beyond the influenced area (from 0° to 90°), Grout can also be injected above the pasted FRP sheet area with a thickness of about 0.2 m to 0.3 m. The grouting process should be adjusted based on field observations of deformations near Tunnel 1 during the excavation of Tunnel 2.

In engineering projects, it is preferable to space the two tunnels out to avoid construction impacts, if possible. If the clear distance between the twin tunnels is less than one tunnel diameter, the nearby construction will have a significant impact on the existing tunnel liner, especially between the tunnel crown and spring line on the second tunnel side (from 90° to 0°). In this case, protective measures are necessary to ensure structural safety and normal operations of the existing tunnel.

4. Conclusions

The paper presented the results of DEM analysis of the construction of shield twin tunnels, performed to assess the impact of the construction of a second tunnel on the first tunnel. The modelled tunnels have diameters of 6.52 m. The analysis was performed using the commonly used DEM software, PFC3D. Displacement, stress variation, porosity variation and coordination of the surroundings of the first tunnel, were assessed. Based on the analysis, the influenced area was determinate. The main conclusions are as follows:

1. The displacement of Tunnel 1 surroundings in horizontal, longitudinal, and vertical directions are larger in the side near the Tunnel 2 excavation area while smaller in the side far away from the excavation area. The horizontal displacements are the largest while the longitudinal displacements are the smallest which can be ignored. The larger displacement zone of Tunnel 1 surroundings is from the angle of 0° to 90°near Tunnel 1 lining.
2. The stresses on the left side of the first tunnel increase, while the stresses on the right side decrease. The excavation of the second tunnel leads to stress relaxation within locations adjacent to the excavation. As a result, compressive stresses increase at locations that are far from the excavation. This indicates that load transfer occurs from the new tunnel to the existing tunnel.
3. Porosity variation corresponds with the displacement changes, in the larger displacement zone, the porosity variation of particles are drastic and become loosen. Coordination changes of Tunnel 1 surroundings can reflect the degree of disturbance of Tunnel 2 excavation, the drastic decrease of coordination in the place of near Tunnel 1 lining indicate the drastic impact of lining and surroundings.
4. In engineering projects, the small distance between tunnel construction and the existing tunnel should be avoided if possible. As the distance between twin tunnels less than the diameter of the tunnel, the nearby construction will give a great influence on the existing tunnel surroundings, especially from the tunnel crown to spring line on the second tunnel side. The protection method is necessary for structure safety and normal operation of the nearby existing tunnel. In this case, the composite reinforcement method consisting of Pasted FRP sheet method and grouting in a specific area can obtain a good protective effect.

Overall, the results showed that the three-dimensional DEM model of the twin tunnels adequately captures the anticipated impacts of the construction of the second tunnel on the first tunnel. However, experimental studies will be necessary to validate the numerical results obtained in this study. Further, additional future analysis should be performed for twin tunnels with larger diameters such as the Wuhan Metro Line 7 tunnels, which have diameters of 15.2 m.

Acknowledgements

The authors wish to thank Professor Daniel Dias from the Grenoble Alpes University, France for his contribution to the paper. The authors would also like to acknowledge the financial support from the National Natural Science Foundation of China (No. 51408450).

ORCID

Lin Wu https://orcid.org/0000-0002-4169-6687
Zhihua Zhang https://orcid.org/ 0000-0003-1583-9311
Weichen Sun https://orcid.org/ 0000-0003-2401-1460

References

Abd-el.rahim HHA, Enieb M, Khalil AA, Ahmed ASH (2015) Twin tunnel configuration for Greater Cairo metro line No. 4. *Computers and Geotechnics* 68:66-77, DOI: 10.1016/j.compgeo.2015.03.015

Addenbrooke TI, Potts DM (2001) Twin tunnel interaction: Surface and subsurface effects. *International Journal of Geomechanics* 1(2): 249-271, DOI: 10.1061/(ASCE)1532-3641(2001)1:2(249)

Arun CO, Rao BN, Srinivasan SM (2010) Stochastic meshfree method for elasto-plastic damage analysis. *Computer Methods in Applied Mechanics and Engineering* 199(37-40):2590-2606, DOI: 10.1016/j.cma.2010.04.009

Chakeri H, Ozcelik Y, Unver B (2015) Investigation of ground surface settlement in twin tunnels driven with EPBM in urban area. *Arabian Journal of Geosciences* 8(9):7655-7666, DOI: 10.1007/s12517-014-1722-2

Chapman DN, Ahn SK, Hunt DV (2007) Investigating ground movements caused by the construction of multiple tunnels in soft ground using laboratory model tests. *Canadian Geotechnical Journal* 44(6):631-

643, DOI: 10.1139/T07-018
Chehade FH, Shahrour I (2008) Numerical analysis of the interaction between twin-tunnels: Influence of the relative position and construction procedure. *Tunnelling and Underground Space Technology* 23(2):210-214, DOI: 10.1016/j.tust.2007.03.004
Chen S, Gui M, Yang MC (2012) Applicability of the principle of superposition in estimating ground surface settlement of twin- and quadruple-tube tunnels. *Tunnelling and Underground Space Technology* 28:135-149, DOI: 10.1016/j.tust.2011.10.005
Chen RP, Wang CJ, Lu L, Meng FY (2017) Influence of excavation on exist metro shield tunnel and control measures. *Engineering Mechanics* 34(12):1-13 (in Chinese)
Chen RP, Zhu J, Liu W, Tang XW (2011) Ground movement induced by parallel EPB tunnels in silty soils. *Tunnelling and Underground Space Technology* 26(1):163-171, DOI: 10.1016/j.tust.2010.09.004
China Fourth Railway Survey and Design Group Co., Ltd. (2013) Preliminary Design Documents of the Yangtze River Tunnel on Sanyang Road of Wuhan Rail Transit Line 7 (In Chinese)
Choi JI, Lee SW (2010) Influence of existing tunnel on mechanical behavior of new tunnel. *KSCE Journal of Civil Engineering*, 14(7):773-783, DOI: 10.1007/s12205-010-1013-8
Cundall PA (1971) A computer model for simulating progressive large scale movements in blocky rock systems. Proceedings of international symposium on rock mechanics, rock fracture, Nancy, France, 2-8
Cundall PA, Strack ODL (1979) A discrete numerical model for granular assemblies. *Géotechnique* 29(1):47-75, DOI: 10.1680/geot.1979.29.1.47
Do NA, Dias D, Oreste P (2015) 3D numerical investigation on the interaction between mechanized twin tunnels in soft ground. *Environmental Earth Science* 73(5):2101-2113, DOI: 10.1007/s12665-014-3561-6
Do NA, Dias D, Oreste P (2016) 3D numerical investigation of mechanized twin tunnels in soft ground – Influence of lagging distance between two tunnel faces. *Engineering Structures* 109:117-125, DOI: 10.1016/j.engstruct.2015.11.053
Do NA, Dias D, Oreste P, Djeran-Maigre I (2014) Three-dimensional numerical simulation of a mechanized twin tunnels in soft ground. *Tunnelling and Underground Space Technology* 42:40-51, DOI: 10.1016//j.tust.2014.02.001
Fang Q, Tai QM, Zhang DL, Wong LNY (2016) Ground surface settlements due to construction of closely-spaced twin tunnels with different geometric arrangements. *Tunnelling and Underground Space Technology* 51:144-151, DOI: 10.1016//j.tust.2015.10.031
Funatsu T, Hoshino T, Sawae H, Shimizu N (2008) Numerical analysis to better understand the mechanism of effects of ground supports and reinforcements on the stability of tunnels using the distinct element method. *Tunnelling and Underground Space Technology* 23(5):561-573, DOI: 10.1016/j.tust.2007.10.003
Hamdia KM, Silani M, Zhuang X, He P, Rabczuk T (2017) Stochastic analysis of the fracture toughness of polymeric nanoparticle composites using polynomial chaos expansions. *International Journal of Frature* 206(2):215-227, DOI: 10.1007/s10704-017-0210-6
He C, Feng K, Fang Y, Jiang YC (2012) Surface settlement caused by twin-parallel shield tunnelling in sandy cobble strata. *Journal of Zhejiang University-SCIENCE A* 13(11): 858-869, DOI: 10.1631/jzus.A12ISGT6
Itasca (2008) Particle flow code in 3 dimensions (PFC3D), user's guide. Itasca Consulting Group, Minneapolis, MN, USA
Jiang MJ, Yin ZY (2012) Analysis of stress redistribution in soil and earth pressure on tunnel lining using the discrete element method. *Tunnelling and Underground Space Technology* 32:251-259, DOI: 10.1016/j.tust.2012.06.001
Jiang MJ, Yin ZY (2014) Influence of soil conditioning on ground deformation during longitudinal tunneling. *Comptes Rendus Mecanique* 342(3):189-197, DOI: 10.1016/j.crme.2014.02.002
Jin DL, Yuan DJ, Li XG, Zheng HT (2018) An in-tunnel grouting protection method for excavating twin tunnels beneath an existing tunnel. *Tunnelling and Underground Space Technology* 71:27-35, DOI: 10.1016/j.tust.2017.08.002
Kim SH (2004) Interaction behaviours between parallel tunnels in soft ground. *Tunnelling and Underground Space Technology* 19(4-5): 448, DOI: 10.1016//j.tust.2004.02.058
Li P, Du SJ, Ma XF, Yin ZY, Shen SL (2014) Centrifuge investigation into the effect of new shield tunnelling on an existing underlying large-diameter tunnel. *Tunnelling and Underground Space Technology* 42:59-66, DOI: 10.1016/j.tust.2014.02.004
Maynar MJM, Rodrigues LE (2005) Discrete numerical model for analysis of earth pressure balance tunnel excavation. *Journal of Geotechnical and Geoenvironmental Eenineering* 131(10):1234-1242, DOI: 10.1061/(ASCE)1090-0241(2005)131:10(1234)
Michel J, Bathaeian SMI, Kuhnert J, Kolymbas D, Chen CH, Polymerou I, Vrettos C, Becker A (2017) Meshfree generalized finite difference methods in soil mechanics — Part II: Numerical results. *GEM - International Journal on Geomathematics* 8(2):191-217, DOI: 10.1007/s13137-017-0096-5
Ming F, Li DQ, Zhang MY, Zhang Y (2017) A novel method for estimating the elastic modulus of frozen soil. *Cold Regions Science and Technology* 141:1-7, DOI: 10.1016/j.coldregions.2017.05.005
Oliaei M, Manafi E (2015) Static analysis of interaction between twin-tunnels using discrete element method (DEM). *Scientia Iranica* 22(6):1964-1971
Ostermann I, Kuhnert J, Kolymbas D, Chen CH, Polymerou I, Smilauer V, Vrettos C, Chen D (2013) Meshfree generalized finite difference methods in soil mechanics — Part I: Theory. *GEM - International Journal on Geomathematics* 4(2):167-184, DOI: 10.1007/s13137-013-0048-7
Qiu JL, Xie YL, Fan HB, Wang ZC, Zhang, YW (2017) Centrifuge modelling of twin-tunnelling induced ground movements in loess strata. *Arabian Journal of Geosciences* 10(22):493, DOI: 10.1007/s12517-017-3297-1
Rabczuk T, Belytschko T (2004) Cracking particles: A simplified meshfree method for arbitrary evolving cracks. *International Journal for Numerical Methods in Engineering* 61(13):2316-2343, DOI: 10.1002/nme.1151
Shahin HM, Nakai T, Ishii K, Iwata T, Kuroi S (2016) Investigation of influence of tunneling on existing building and tunnel: Model tests and numerical simulations. *Acta Geotechnica* 11(3):679-692, DOI: 10.1007//s11440-015-0428-2
Vu-Bac N, Lahmer T, Zhuang X, Nguyen-Thoi T, Rabczuk T (2016) A software frameword for probalistic sensitivity analysis for computationally expensive models. *Advances in Engineering Software* 100:19-31, DOI: 10.1016/j.advengsoft.2016.06.005
Wang J, He C, Wang C, Chen Z Q, Tang R (2018) Face stability analysis of EPB shield tunnel in sand. *Chinese Journal of Geotechnical Engineering* 40(1):1-9 (in Chinese)
Wang MN, Wei LH, Lu JF, Zhu ZG (2011) Study of face stability of cobble-soil shield tunneling at Chengdu metro. *Rock and Soil Mechanics* 32(1):99-105 (in Chinese)
Yu LP (2014) Analysis of soil's elastic modulus values based on FLAC^{3D} simulation. *Journal of Water Resources and Architectural Engineering* 12(2):162-166 (in Chinese)

Zhang ZX, Hu XY, Scott KD (2011) A discrete numerical approach for modeling face stability in slurry shield tunnelling in soft soils. *Computers and Geotechnics* 38(1):94-104, DOI: 10.1016/j.compgeo.2010.10.011

Zhang ZH, Zhang XD, Tang Y, Cui YF (2018) Discrete element analysis of a cross-river tunnel under random vibration levels induced by trains operating during the flood season. *Journal of Zhejiang University-SCIENCE A* 19(5):346-366, DOI: 10.1631/jzus.A1700002